MORPHOLOGICAL AND OPTICAL PROPERTIES OF ELECTROSPUN SnO$_2$ FIBERS

A. D. BUSUIOC[a], I. CIOVICĂ[a], Ş. STOLERIU[a], M. ENCULESCU[b*],
A. EVANGHELIDIS[b], T. VIŞAN[a]
[a]University POLITEHNICA of Bucharest, RO-011061, Bucharest, Romania
[b]National Institute of Materials Physics, RO-077125, Magurele, Romania

The electrospinning technique was employed for the preparation of SnO$_2$ fibers starting from a precursor solution consisting of a tin salt, polyvinylpyrrolidone as carrier polymer and N,N-dimethylformamide as dispersion medium. In order to achieve single-phase crystalline structures, the as-spun fibers were calcined at 500, 700 or 900 °C, with two different heating rates of 1 or 10 °C/min. The thermally treated samples were characterized in terms of structure, morphology and bandgap by employing X-ray diffraction, scanning electron microscopy coupled with energy-dispersive X-ray spectroscopy and UV-Vis spectroscopy. A fine tuning of the bandgap width was attained through the selection of different values for the electrospinning and calcination parameters.

1. Introduction

Gas sensors have demonstrated over the past decades their importance in monitoring certain types of gases in real time and in a continuous manner, to ensure safety against gas-generated hazards, for environmental or human protection [1]. The requirements that these types of devices have to meet are as follows: high sensitivity, gas selectivity, chemical stability, short response and recovery times, low operating temperature and power consumption, reduced size, low cost and extended lifetime [2].

Metal oxides have a considerable potential as candidates for the emerging technologies, including fields such as: optics, electronics, optoelectronics and biology [3-6]. The performances of the corresponding systems depend on the size, shape and surface of the active material [7, 8]. In other words, the optical and electrical properties of oxides are strongly influenced by the chemical composition, crystalline structure and morphological features of the approached structures.

Moreover, the physical and chemical properties of oxide materials dramatically change in a positive way when their dimension switch from the macro and micro fields to the nano one. Structures like: nanoparticles [9], nanowires [10], nanorods [11], nanofibers [12-14], nanotubes [15], nanobelts [16] and thin films [17], are of high interest. A further improvement of the functional properties is possible through doping [18], loading [19] or integration in complex composites [20].

Tin dioxide (SnO$_2$) is an *n* type semiconductor with a bandgap width of 3.6 eV [8, 21]. Due to its unique characteristics, among which the transparency and conductivity are the most notable, nanostructured SnO$_2$ represents a choice for both researcher and engineers, regarding the development of sensing devices for a wide range of gases [12, 13, 18, 20, 22, 23]. It is also employed for other types of applications, such as solar cells [24, 25], ion batteries [14, 26], photocatalysts [27, 28] and biosensors [19, 29].

The synthesis of one-dimensional materials based on SnO$_2$ has been performed especially through the electrospinning technique [11-13, 15, 18-20, 22, 23, 30], which is a simple, versatile and environmental friendly approach for the fabrication of polymeric or inorganic fibers [31].

*Corresponding author: mdatcu@infim.ro

Briefly, the precursor solution containing at least a polymer and a solvent is pumped in a high electric field and, as a function of the equipment configuration, random or ordered nonwoven mashes are deposited on the collector. Several carrier polymers have been used for the preparation of SnO_2 structures, such as: polyvinylpyrrolidone [12-14, 18, 20, 22, 23, 30], polyvinyl alcohol [13], polyacrylonitrile [32] or polyvinyl acetate [33].

In this work, we report on the synthesis and characterization of SnO_2 fibers obtained through the electrospinning method. The precursor solution was electrospun in optimized conditions and the resulting one-dimensional structures were subjected to a thermal treatment in the 500 - 900 °C range. The heating rate was modified in order to investigate the influence of this processing parameter on the morphological and optical properties of the semiconductor oxide fibers.

2. Experimental

SnO_2 fibers were prepared by the electrospinning technique, using tin(II) chloride dihydrate ($SnCl_2 \cdot 2H_2O$, ≥ 98 %, Sigma-Aldrich), polyvinylpyrrolidone (PVP, MW ~ 1,300,000, Aldrich) and N,N-dimethylformamide (DMF, ≥ 99,8 %, Sigma-Aldrich). If the first compound represents the source of metallic cations, the other two are used only as sacrificial substances, namely as carrier polymer for generating an appropriate viscosity of the solution (PVP) and solvent for the dissolution of the solid starting materials (DMF). The electrospinning solution was obtained by solubilizing 8 g of $SnCl_2 \cdot 2H_2O$ and 4 g of PVP in 25 mL of DMF and stirring at room temperature for at least 2 h. At the end of the homogenization step, a light yellow solution was achieved, whose color turns in several hours to a more intense yellow, probably due to the partial oxidation of tin cations ($Sn^{2+} \rightarrow Sn^{4+}$). Further, the precursor solution was loaded in a plastic syringe with a blunt tipped stainless steel needle having 0.8 mm interior diameter. The syringe was connected to a syringe pump, which feeds the equipment with a constant flow. A positive voltage was applied to the needle, so that to make possible the solution spinning and fibers deposition on the grounded collector, placed at a fixed distance from the tip of the needle. The one-dimensional structures were gathered on silicon substrates. After optimizing the electrospinning conditions, the following values were chosen: 0.5 mL/h feeding rate, 15 kV applied voltage and 15 cm working distance.

The next step consisted in the calcination of the as-spun samples in order to cause the elimination of the organic components, as well as nucleation and growth of SnO_2 crystals. The thermal treatment parameters were: 1 or 10 °C/min heating rate, 500, 700 or 900 °C maximum temperature and 2 h period at the mentioned temperatures.

A thermal analysis on the precursor fibers was necessary to identify the temperature at which the organic part is completely removed; this was performed on a Shimadzu DTG-60 equipment, in the 25 - 1000 °C temperature range. The calcined fibers were investigated by X-ray diffraction (XRD), scanning electron microscopy (SEM) coupled with energy-dispersive X-ray spectroscopy (EDX) and UV-Vis spectroscopy. A Shimadzu XRD 6000 diffractometer with Ni filtered Cu Kα radiation (λ = 0.154 nm), 2θ ranging between 20 and 80 °, was used for the structural characterization, while a Quanta Inspect F scanning electron microscope was employed to visualize the morphology. The reflectance spectra in the UV-Vis field were recorded with two different equipments, as a function of the amount and features of the specimens (small quantity uniformly dispersed on the substrate or high quantity intensely exfoliated from the substrate). Thus, a Perkin Elmer Lambda 45 UV-Vis spectrophotometer equipped with an integrating sphere was used for the first case and a Jasco V 560 UV-Vis spectrophotometer for the second one. In order to estimate the bandgap values, Kubelka-Munk functions ($F(R)$) were calculated on the basis of the reflectance data and $[F(R) \cdot E]^2$ functions were plotted versus photon energy (E); Kubelka-Munk function is expressed as $F(R)=(1-R)^2/(2 \cdot R)$, where R is the observed diffuse reflectance.

3. Results and discussion

The precursor fibers containing both the mineral and organic components were subjected to thermal analysis from room temperature to 1000 °C, in air. As it can be identified on the TG curve (Fig. 1), the material suffers a significant weight loss of about 57 % up to 450 °C. Namely, below 110 °C, a small weight loss associated with an endothermic effect is present, the process being identified as the evaporation of residual solvent and moisture. Further, two important weight losses with maxima at approximately 300 and 418 °C, coupled with an intense and extensive exothermic effect, can be assigned to PVP combustion and chlorine elimination, simultaneously with Sn^{2+} oxidation and SnO_2 crystallization. At higher temperatures, a better arrangement of the ions in the crystalline network is possible. The total weight loss in the studied range was calculated as 69 %, the decrease occurred above 450 °C being determined by the air flow in the equipment; this trains a part of the loose and light mass from the measuring crucible. In conclusion, the minimum temperature at which the as-spun fibers should be calcined in order to achieve oxide structures is 500 °C, higher values influencing especially the structural features and grain dimension.
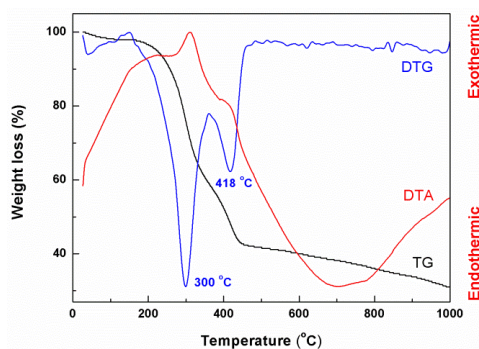

Fig. 1. Thermal analysis performed on the as-spun fibers: TG - thermogravimetric analysis, DrTGA - the derivative of the themogravimetric analysis with respect to time and DTA - differential thermal analysis

Going to the morphology of the precursor fibers, Figs. 2 a and a' display their overall aspect, as well as the thickness and length. The resulted one-dimensional structures are deposited on the substrate randomly, in the form of a nonwoven mesh, and present an uniform thickness over the entire length. Based on the analysis of several SEM images, the average thickness was estimated to about 400 nm, while the length can reach even hundreds of nm.

The EDX spectra recorded on both as-spun and 500 °C calcined samples (Fig. 2 b) show the elemental composition and its evolution after the applied thermal treatment. It is obvious that Cl^- is completely removed from the system even for the lowest calcination temperature. C is still present in the case of the thermally treated fibers due to the tape employed for fixing the specimens, while Au was used as conductive coating.
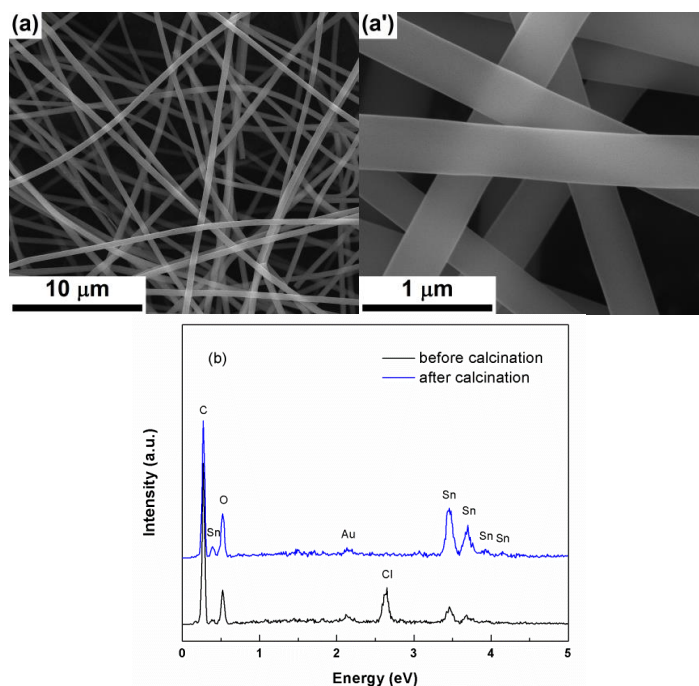
*Fig. 2. SEM images of the as-spun fibers (a and a') and EDX spectra of
the fibers before and after calcination at 500 °C (b).*

The thermal process allowed the obtaining of SnO_2 with rutile-like structure (tetragonal symmetry, JCPDS 01-080-6727) as single-phase. As indicated in Fig. 3, the emerged maxima are attributed either to the deposited material or to the substrate. The growth of the calcination temperature led, as expected, to the increase of the crystallinity degree, as well as to larger crystallites, fact proved by the narrower and more intense peaks. A quick assessment of the average crystallite size with Scherrer equation revealed a doubling of this parameter from 500 to 900 °C.
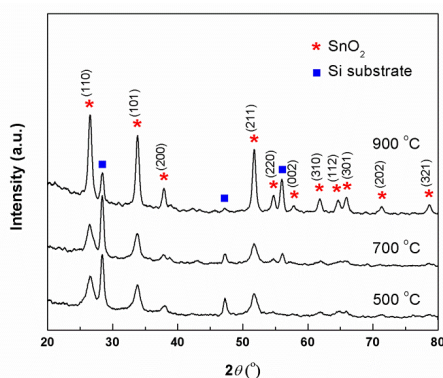

Fig. 3. XRD patterns of SnO_2 calcined fibers for 1 °C/ min heating rate.

Figs. 4 and 5 present the SEM images at two magnifications for SnO_2 fibers thermally treated in different conditions. For all samples, a reduction of about 25 % in diameter can be noticed, explained on the basis of organic part combustion, while the dimensional uniformity is maintained. The processes of nucleation, growth and densification of the oxide phase are governed by different laws, as a function of calcination temperature and heating rate. For 1 °C/min (Fig. 4), the fibers are made up of quasi-spherical grains, whose average size increases with temperature increasing from less than 20 nm (500 °C - Figs. 4 a and a') to approximately 40 nm (700 °C - Figs.

4 b and b') and 50 nm (900 °C - Figs. 4 c and c'). Moreover, a porosity enhancement can be observed, in the sense of bigger pores occurrence, due to material diffusion in order to promote larger grains during the long thermal treatment, without fiber diameter reduction.
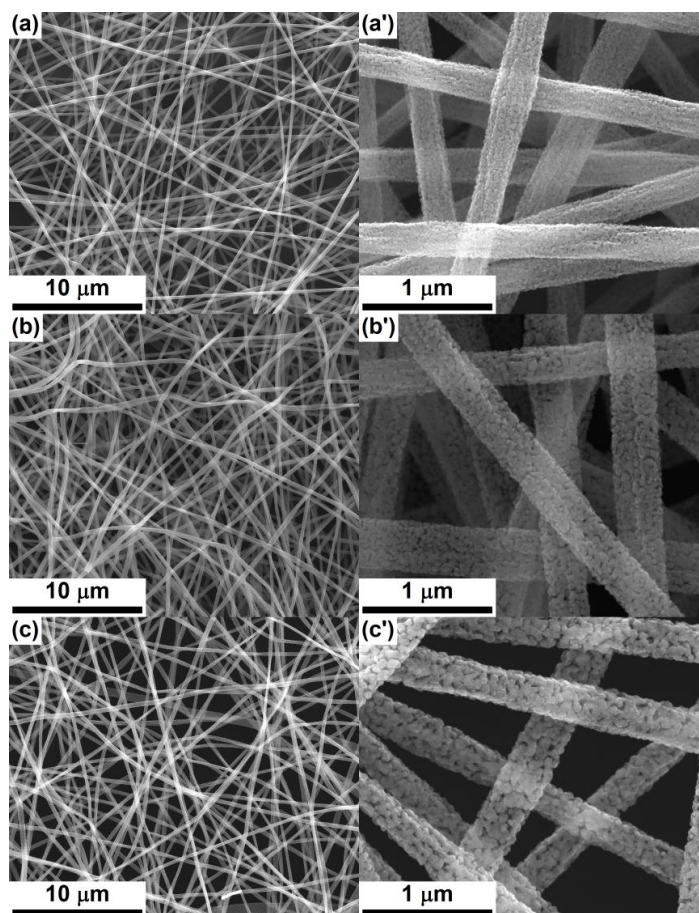
Fig. 4. SEM images of SnO$_2$ fibers calcined at: 500 °C (a and a'), 700 °C (b and b') and 900 °C (c and c'), for 1 °C/ min heating rate

The acceleration of heating (10 °C/min, Fig. 5) causes important modifications regarding morphology. Thus, the low magnification SEM images indicate a pronounced fragility of SnO$_2$ fibers, especially for 500 °C calcination temperature, probably because of the violent removal of PVP from the volume of the structures, which leads to an unstable architecture, with the tendency to collapse under its own weight. The increase of the temperature to 700 or 900 °C has a positive effect on the fiber resistance structure, so that the cases of material breakage are fewer or even nonexistent. A higher heating rate inhibits the grain growth, the average dimension being below 20 nm for 500 °C (Figs. 5 a and a'), around 30 nm for 700 °C (Figs. 5 b and b') and 40 nm for 900 °C (Figs. 5 c and c'). In conclusion, by changing the values of the thermal treatment parameters, the morphology of SnO$_2$ fibers can be precisely controlled, aspect that subsequently influences the optical and electrical properties.
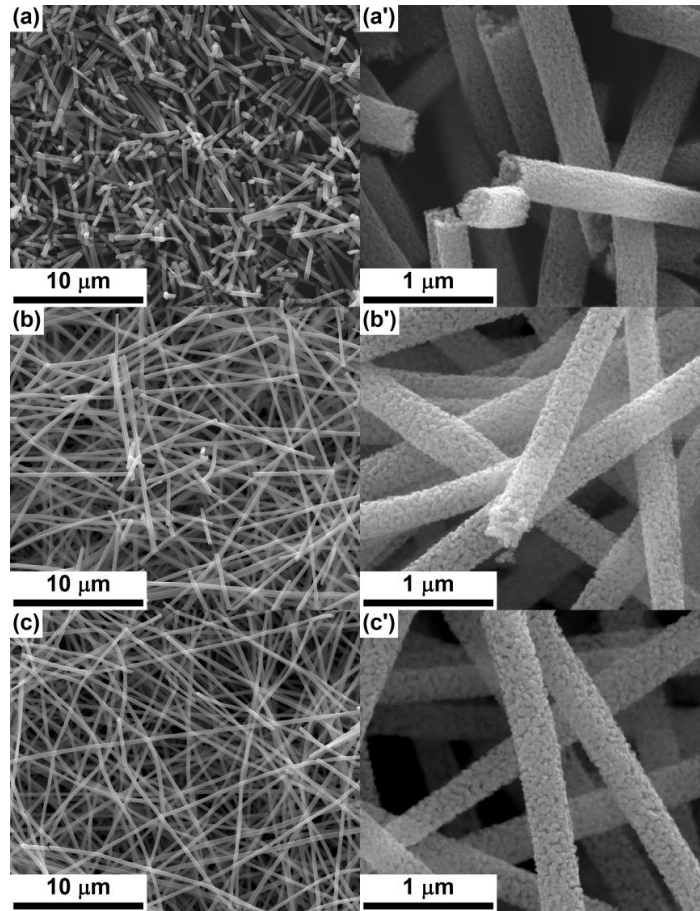
Fig. 5. SEM images of SnO$_2$ fibers calcined at: 500 °C (a and a'), 700 °C (b and b') and 900 °C (c and c'), for 10 °C/ min heating rate.

Starting from the UV-Vis spectra of the calcined fibers (Figs. 6a and 7a) and employing Kubelka-Munk graphical representations (Figs. 6b and 7b), the values of the bandgap were extracted and the results are displayed in Fig. 8.
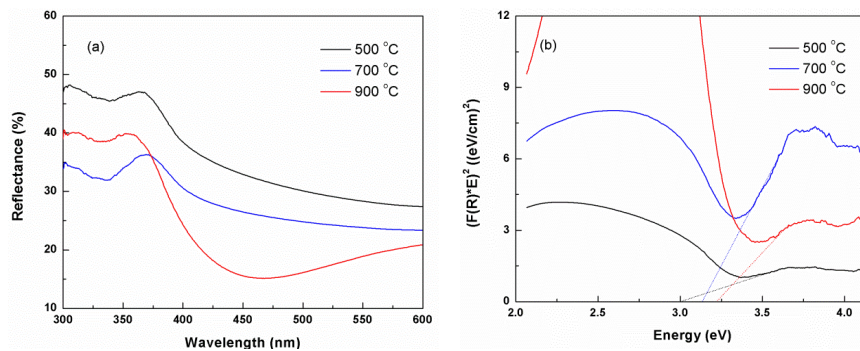

Fig. 6. Reflectance spectra (a) and representation of Kubelka-Munk functions (b) for SnO$_2$ calcined fibers with 1 °C/ min heating rate.
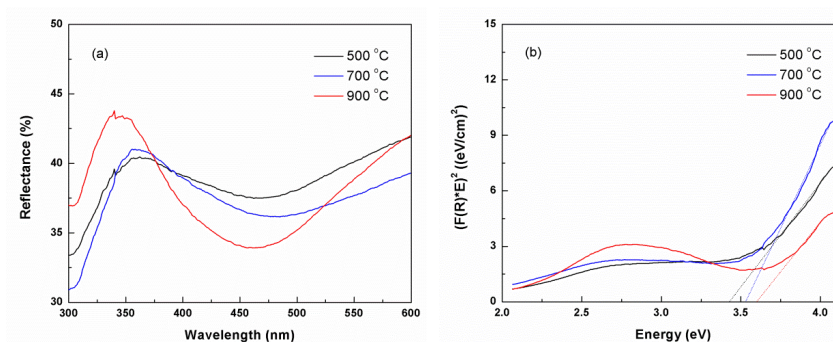
Fig. 7. Reflectance spectra (a) and representation of Kubelka-Munk functions (b) for SnO$_2$ calcined fibers with 10 °C/ min heating rate.

The bandgap width increases with calcination temperature raising due to an expected improvement of the crystalline network ordering, accompanied with a reduction of defects concentration. Moreover, a lower heating rate promotes smaller bandgap values, in correlation with material evolution from structural and ceramic point of view. Taking into account the trend of the average crystallite size and average grain size with the processing conditions (Figs. 3, 4 and 5), the band gap shift could be attributed to a size effect [34].
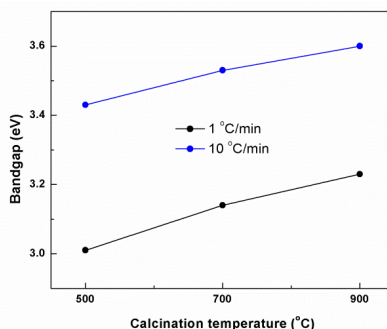

Fig. 8. Variation of the bandgap values as a function of the temperature and heating rate of the calcination for SnO$_2$ fibers

4. Conclusions

SnO$_2$ fibers were successfully synthesized through a two-step procedure: electrospinning, followed by calcination in the 500 - 900 °C temperature range; the heating rate was increased from 1 to 10 °C/min in order to investigate its influence on the morphological and optical characteristics. The conversion of the precursor fibers in oxide ones is accompanied by a diameter reduction of about 25 %.

An unique oxide phase with rutile-like structure, specific to SnO$_2$, was identified in the thermally treated samples. The grain size and porosity vary as a function of the calcination temperature, but especially of the heating rate.

The bandgap values, estimated on the basis of the UV-Vis reflectance spectra, were within the range 3.0 - 3.6 eV, which highlights the possibility of optical properties tuning to a large extent without employing additives or dopants. Thus, SnO$_2$ fibers suitable for gas sensor applications can be obtained in the case of a low calcination temperature and a small heating rate.

Such one-dimensional structures can be easily integrated in nanoscale devices for the field of advanced sensors, the optical properties being directly determined by the structural and morphological properties of the active material, which can be accurately modified via the processing conditions.

Acknowledgements

References

[1] G. Eranna; Metal oxide nanostructures as gas sensing devices; CRC Press, 2012.

[2] X. Liu, S. Cheng, H. Liu, S. Hu, D. Zhang, H. Ning; Sensors **12**, 9635 (2012).

[3] M. Enculescu, A. Evanghelidis, C. Busuioc, C. Florica, A. Costas, M. Oancea, N. Preda, E. Matei, I. Enculescu; Digest Journal of Nanomaterials and Biostructures **9**, 809 (2014).

[4] C. Busuioc, A. Evanghelidis, C. Florica, I. Enculescu; Digest Journal of Nanomaterials and Biostructures **9**, 1569 (2014).

[5] C. Busuioc, A. Evanghelidis, A. Galatanu, I. Enculescu; Scientific Reports **6**, 34584 (2016).

[6] M. Beregoi, C. Busuioc, A. Evanghelidis, E. Matei, F. Iordache, M. Radu, A. Dinischiotu, I. Enculescu; International Journal of Pharmaceutics **510**, 465 (2016).

[7] M. Batzill, U. Diebold; Progress in Surface Science **79**, 47 (2005).

[8] S. Das, V. Jayarman; Progress in Materials Science **66**, 112 (2014).

[9] H. Kose, S. Karaal, A.O. Aydin, H. Akbulut; Materials Science in Semiconductor Processing **38**, 404 (2015).

[10] C.M. Liu, X.T. Zu, Q.M. Wei, L.M. Wang; Journal of Physics D **39**, 2494 (2006).

[11] J. Zhu, G. Zhang, S. Gu, B. Lu; Electrochimica Acta **150**, 308 (2014).

[12] X.X. Fan, X.L. He, J.P. Li, X.G. Gao, J. Jia; Vacuum **128**, 112 (2016).

[13] E. Nikan, A.A. Khodadadi, Y. Mortazavi; Sensors and Actuators B **184**, 196 (2013).

[14] Z. Huang, H. Gao, Q. Wang, Y. Zhao, G. Li; Materials Letters **186**, 231 (2017).

[15] L. Cheng, S.Y. Ma, T.T. Wang, X.B. Li, J. Luo, W.Q. Li, Y.Z. Mao, D.J. Gz; Materials Letters **131**, 23 (2014).

[16] L. Li, K. Yu, J. Wu, Y. Wang, Z. Zhu; Crystal Research and Technology **45**, 539 (2010).

[17] E. Preiss, T. Rogge, A. Krauss, H. Seidel; Procedia Engineering **120**, 88 (2015).

[18] X. Kou, C. Wang, M. Ding, C. Feng, X. Li, J. Ma, H. Zhang, Y. Sun, G. Lu; Sensors and Actuators B **236**, 425 (2016).

[19] S. Liu, B. Yu, F. Li, Y. Ji, T. Zhang; Electrochimica Acta **141**, 161 (2014).

[20] Y. Zhao, X. He, J. Li, X. Gao, J. Jia; Sensors and Actuators B **165**, 82 (2012).

[21] R. Barik, N. Devi, D. Nandi, S. Siwal, S.K. Ghosh, K. Mallick; Journal of Alloys and Compounds **723**, 201 (2017).

[22] S.W. Choi, A. Katoch, G.J. Sun, S.S. Kim; Sensors and Actuators B **181**, 787 (2013).

[23] S.H. Yan, S.Y. Ma, X.L. Xu, W.Q. Li, J. Luo, W.X. Jin, T.T. Wang, X.H. Jiang, Y. Lu, H.S. Song; Materials Letters **159**, 447 (2015).

[24] E.M. Jin, J.Y. Park, H.B. Gu, S.M. Jeong; MaterialsLetters **159**, 321 (2015).

[25] I.M.A. Mohamed, V.D. Dao, A.S. Yasin, H.S. Choi, N.A.M. Baraka; International Journal of Hydrogen Energy **41**, 10578 (2016).

[26] A.K. Haridas, C.S. Sharma, N.Y. Hebalkar, T.N. Rao; Materials Today Energy **4**, 14 (2017).

[27] X. Wang, H. Fan, P. Ren; Catalysis Communications **31**, 37 (2013).

[28] C. Zhu, Y. Li, Q. Su, B. Lu, J. Pan, J. Zhang, E. Xie, W. Lan; Journal of Alloys and Compounds **575**, 333 (2013).

[29] Y.E. Miao, S. He, Y. Zhong, Z. Yang, W.W. Tjiu, T. Liu; Electrochimica Acta **99**, 117 (2013).

[30] B.R. Koo, S.T. Oh, H.J. Ahn; Materials Letters 178, 288 (2016).

[31] A. Macagnano, E. Zampetti, E. Kny; Electrospinning for High Performance Sensors; Springer, 2015.

[32] A.B. Suryamas, G.M. Anilkumar, S. Sago, T. Ogi, K. Okuyama; Catalysis Communications **33**, 11 (2013).

[33] A. Katoch, J.H. Byun, S.W. Choi, S.S. Kim; Sensors and Actuators B **202**, 38 (2014).

[34] C. Busuioc, A. Evanghelidis, M. Enculescu, I. Enculescu; Digest Journal of Nanomaterials and Biostructures **10**, 957 (2015).